Synergistic Enhancement of Sludge Deep-Dewatering via Tea Waste and Sludge-Derived Biochars Coupled with Polyaluminum Chlorid

Qiang-Ying Zhang , Geng Xu , Hui-Yun Qi , Xuan-Xin Chen , Hou-Feng Wang * , Xiaomei Cui *

Posted Date: 23 July 2025

doi: 10.20944/preprints202507.1948.v1

Keywords: biochar-based conditioning; sludge dewatering; polyaluminum chloride (PAC); tea waste biochar; pore structure reconstruction

 doi:10.20944/preprints202507.1948.v1

Article

Synergistic Enhancement of Sludge Deep-Dewatering via Tea Waste and Sludge-Derived Biochars Coupled with Polyaluminum Chlorid

Qiang-Ying Zhang [1], Geng Xu [1], Hui-Yun Qi [2], Xuan-Xin Chen [2], Hou-Feng Wang [2,*] and Xiao-Mei Cui [1,*]

[1] Key Laboratory of Biodiversity and Environment on the Qinghai-Tibet Plateau, Ministry of Education, School of Ecology and Environment, Tibet University, Lhasa 850000, China.

[2] Fujian Provincial Key Laboratory of Soil Environmental Health and Regulation, College of Resources and Environment, Fujian Agriculture and Forestry University, Fuzhou 350002, China

* Correspondence: wanghf@mail.ustc.edu.cn (H.F.W.); cuixiaomei@utibet.edu.cn (X.M.C.); Tel.: +86 0591-86399045 (H.F.W.); Tel.: +86 0891-6657598) (X.M.C.)

Abstract

Although coagulation can enhance sludge dewatering performance, it often leads to dense flocs, hindered water release, and secondary pollution of the sludge cake. In this study, three types of biochar-based skeleton materials：tea waste-derived biochar (TB), PAC sludge-derived biochar (PB), and their mixture (MB) were employed in combination with polyaluminum chloride (PAC) to improve sludge permeability and water release capacity. Results showed that PAC alone reduced the water content (Wc) and capillary suction time (CST) of raw sludge (RS) from 79.07% and 97.45 s to 69.45% and 42.30 s, respectively. In contrast, biochar-PAC composite conditioning achieved further enhancement. Among them, the TBP group (10% DS TB + 40 mg/g SS PAC) exhibited the best performance, with Wc and CST reduced to 58.73% and 55.65 s, reaching the threshold for deep dewatering (Wc < 60%). Low-field nuclear magnetic resonance (LF-NMR) analysis revealed an enhanced transformation from bound to free water, improving water mobility. Zeta potential and particle size analysis indicated that biochar promoted electrostatic neutralization and adsorption bridging. Rheological and EPS measurements demonstrated significant reductions in yield stress and apparent viscosity, alongside enhanced release of proteins and polysaccharides into soluble EPS (S-EPS). Scanning electron microscopy and pore structure analysis further confirmed that biochar formed a stable porous skeleton (pore diameter up to 1.365 μm), improving sludge cake permeability. In summary, biochar synergizes with PAC through a "skeleton support–charge neutralization–adsorption bridging" mechanism, reconstructing sludge microstructure and significantly improving deep dewatering performance.

Keywords: biochar-based conditioning; sludge dewatering; polyaluminum chloride (PAC); tea waste biochar; pore structure reconstruction

1. Introduction

In recent years, the rapid global expansion of wastewater treatment has driven a continuous increase in the production of waste activated sludge (WAS)[1]. In China alone, the annual municipal sludge output exceeded 60 million tons (calculated at 80% moisture content) in 2024, with industry forecasts suggesting it may approach 160 million tons by 2025, driven by rising urban water reuse rates and the expansion of rural wastewater treatment infrastructure[2,3]. The high moisture content of sludge not only leads to soaring costs in transportation, landfilling, and incineration, but also results in the accumulation of pathogens, persistent organic pollutants, and heavy metals, thereby exerting dual pressure on ecological health and carbon mitigation[4]. Both engineering practice and

 doi:10.20944/preprints202507.1948.v1

policy experience have demonstrated that maintaining the filter cake moisture content (Wc) below 60% is a necessary precondition for achieving volume reduction, hygienization, and energy recovery[5,6]. Consequently, the development of safe, efficient, and environmentally friendly deep dewatering technologies has become a central focus in terminal sludge treatment[7,8].

Coagulation conditioning, dominated by an "electrostatic neutralization–adsorptive bridging" mechanism, is the most widely applied approach in sludge dewatering, with polyaluminum chloride (PAC) regarded as an industry benchmark owing to its low cost and broad pH tolerance[9,10]. Nevertheless, extensive literature and field experience demonstrate that exclusive coagulation often produces densely packed flocs that hinder water transport pathways, falling short of deep-dewatering requirements[8,11]. Moreover, the aluminum-rich cakes produced by PAC can release secondary pollutants during incineration or land application, raising public and regulatory concerns[12]. To overcome these bottlenecks, researchers have introduced a "skeleton-building"strategy that incorporates rigid, porous particles to create a stable support network within the floc matrix, thereby lowering compressibility and accelerating water migration[8,13,14].

Inorganic skeleton materials such as fly ash, diatomite, red mud, and lime have demonstrated the ability to reduce Wc to approximately 50% due to their high porosity and mechanical strength[3,15–17]. However, these materials typically require high dosages, ranging from 20–50% of the dry solid (DS) content. Excessive addition of inorganic skeletons significantly increases the ash content of the filter cake, thereby reducing its calorific value during incineration[16]. Furthermore, concerns have been raised regarding the potential leaching of heavy metals from fly ash and red mud, while the high alkalinity of lime can inhibit microbial activity during subsequent anaerobic digestion, limiting its land application potential[18,19]. These hidden environmental and economic costs have prompted the search for greener, low-dosage alternatives to conventional skeleton materials.

Biochar, derived from the pyrolysis of agricultural residues or sewage sludge, has emerged as a promising alternative due to its multi-scale porosity, high specific surface area, and abundant oxygen-containing functional groups[20,21]. Biochar can achieve comparable dewatering enhancement to inorganic skeletons at low dosages (≤10% DS), while also offering carbon-negative attributes, low toxicity, and resource recovery potential[22]. Recent studies have shown that the pore size distribution of biochar (1 nm–100 μm) is highly compatible with the colloidal particle sizes in sludge, providing open water transport pathways[23,24]. Moreover, surface carboxyl and hydroxyl groups on biochar can form synergistic adsorption-bridging interactions with PAC, enhancing charge neutralization[25,26]. The pyrolytic process also stabilizes heavy metals, reducing environmental risks during downstream utilization[14]. Among biochar sources, tea stems, a byproduct of tea processing with an annual production exceeding 600,000 tons in China[27], can yield biochar (TB) with a honeycomb-like porous network (0.8–1.3 μm pore size) and high compressive strength (>3 MPa)[28]. However, current research has primarily focused on the chemical adsorption properties of TB, with limited attention to its potential as a physical skeleton material[27]. More innovatively, blending TB with PAC-derived sludge-based biochar (PB) to form a mixed biochar (MB) may offer dual functionalities, lightweight structural support from TB and intrinsic aluminum/iron-based charge neutralization from PB, thus establishing a "mechanical–electrochemica" bifunctional skeleton for deep dewatering applications.

To date, studies on the "tea-branch biochar–PAC"synergy have remained at the performance level, lacking systematic elucidation of multiscale mechanisms such as charge regulation, EPS migration, and pore-network reconstruction. In this work, tea-branch biochar (TB), PAC sludge biochar (PB), and their mixture (MB) were selected as representative skeleton materials. Through individual and combined dosing experiments with PAC, we comprehensively evaluated their impacts on the deep-dewatering efficiency of municipal sludge and, using zeta-potential analysis, rheology, EPS fractionation, and SEM–XCT-based pore-network reconstruction, unraveled the collaborative "skeleton support–electrostatic neutralization–EPS reconfiguration" mechanism. This study not only provides theoretical support for the high-value utilization of tea-processing waste but

 doi:10.20944/preprints202507.1948.v1

also offers practical guidance for developing resource-friendly, low-carbon, and high-efficiency deep-dewatering technologies for sludge management.

2. Materials and Methods

2.1. Sludge Samples and Chemical Reagents

Raw sludge (RS) was collected from the secondary sedimentation tank of the Jinshan Wastewater Treatment Plant in Fuzhou, Fujian Province, China. After sampling, the sludge was allowed to settle for 6–8 hours to remove the supernatant, then sieved through an 80-mesh stainless steel screen, and stored at 4 °C for no more than 7 days[29]. The basic physicochemical properties of the raw sludge are summarized in Table 1. Tea processing residues were obtained from Wuyishan, Fujian Province. Analytical-grade polyaluminum chloride (PAC, $Al_2O_3 \geq 29$ %) was purchased from Chengdu Aikeda Chemical Reagent Co., Ltd. All other chemicals used were of analytical grade.

Table 1. The characteristics of the raw activated sludge employed in the experiments.

Parameter	value
Moisture content (%)	97.77±0.06
pH	6.98±0.27
Zeta potential (mV)	-25.20±1.55
Dry solids (g/L)	22.30±0.24
Volatile solids (g/L)	11.80±0.10
CST (s)	97.45±1.90

2.2. Biochar Preparation

(1) Tea-branch biochar (TB): Tea branches were dried at 70 °C, ground to pass through a 100-mesh sieve, and pyrolyzed at 500 °C for 2 h under a nitrogen atmosphere (100 mL min^{-1}). After natural cooling, the biochar was sieved to 80–250 μm.

(2) PAC sludge-derived biochar (PB): Sludge cakes conditioned with PAC at a dosage of 60 mg g^{-1} SS were dried in an oven at 105 °C, pulverized to pass through a 100-mesh sieve, and pyrolyzed using the same conditions as for TB.

(3) Mixed biochar (MB): The powdered TB and aluminum-rich sludge biochar (PB) were thoroughly mixed in a mass ratio of 1:2 and subjected to the same pyrolysis procedure described for TB, yielding MB.

2.3. Sludge Conditioning and Dewatering Tests

Homogenized sludge (500 mL) was added to a 600 mL beaker and stirred at 300 rpm for 3 min to serve as the blank (RS). Control groups were conditioned with either TB, PB, or MB at dosages of 5, 10, 15, or 20 % DS, and PAC at 40 mg g^{-1} SS, using identical stirring conditions. For combined conditioning, a two-step method was applied: PAC (40 mg g^{-1} SS) was first added and pre-mixed for 3 min, followed by the addition of 10 % DS biochar and an additional 3 min of stirring. The resulting samples were labeled TBP, PBP, and MBP. All experiments were conducted in triplicate. Detailed parameters are provided in Table 2.

Dewatering performance was assessed using capillary suction time (CST, Trion Model 319) and filter cake water content (Wc). Samples were filtered under a constant pressure of 0.8 MPa for 30 min. The resulting filter cakes were dried at 105 °C for 24 h and weighed. Wc was calculated as the mass percentage of water in the total filter cake[30]. Each test was performed in triplicate, and mean values were used for analysis.

2.4. Water State Characterization and Multiscale Analysis

Sludge samples subjected to different pretreatments were placed in 18 mm glass tubes and analyzed using a PQ001 low-field nuclear magnetic resonance (LF-NMR) spectrometer (32 MHz,

 doi:10.20944/preprints202507.1948.v1

32 °C). CMPG sequences were collected using an echo time of 0.2 ms, 5000 echoes, 8 scans, and a sampling rate of 200 kHz[31,32].

Subsequently, surface functional groups of the three types of biochar were analyzed by Fourier-transform infrared spectroscopy (FTIR; Nicolet iS50, KBr pellets, resolution 4 cm^{-1}, range 400–4000 cm^{-1}). Crystalline phases were identified using X-ray diffraction (XRD; Rigaku Ultima IV, Cu Kα, 40 kV, 40 mA, scan range 5°–80°, scan rate 1° min^{-1}). Specific surface area and pore size distribution were measured using nitrogen adsorption–desorption (ASAP 2460; degassed at 250 °C for 8 h, analyzed using the NLDFT model). Microstructural morphology was observed by scanning electron microscopy (SEM; Hitachi SU8020, 10 kV, Au sputter-coated) at magnifications ranging from 10,000× to 30,000×.

Table 2. Different sludge conditioning procedures.

Sample	Conditioning reagents	Dosage		Conditioning process
		PAC (mg/g SS)	Biochars (% DS)	
RS	-	-	-	-
PAC	PAC	40	-	After adding PAC solution, the mixture was stirred at 300 rpm for 3 min.
TB-5	TB	-	5	After adding different doses of tea stem biochar, the mixture was stirred at 300 rpm for 3 min.
TB-10		-	10	
TB-15		-	15	
TB-20		-	20	
PB-5	PB	-	5	After adding different doses of aluminum-based mud biochar, the mixture was stirred at 300 rpm for 3 min.
PB-10		-	10	
PB-15		-	15	
PB-20		-	20	
MB-5	MB	-	5	After adding different doses of mixed biochar, the mixture was stirred at 300 rpm for 3 min.
MB-10		-	10	
MB-15		-	15	
MB-20		-	20	
TBP	PAC、TB	40	10	PAC solution was added first and stirred at 300 rpm for 3 min, and then biochar was added and stirred at 300 rpm for 3 min;
PBP	PAC、PB			
MBP	PAC、MB			

2.5. Physicochemical and Biochemical Characterization of Sludge

The electrokinetic and rheological properties of the sludge were characterized using both the supernatant and whole sludge. After centrifugation at 3000 × g for 5 min, the supernatant was analyzed at 25 °C for zeta potential using a zeta potential analyzer (Beckman Coulter Delsa™ Nano). Floc size distribution was measured using a Malvern MS2000 laser particle size analyzer (Malvern Instruments Ltd, London, UK), with six replicates per sample.

Extracellular polymeric substances (EPS) were sequentially extracted using a modified thermal extraction protocol to obtain S-EPS, LB-EPS, and TB-EPS[33]. Protein and polysaccharide concentrations were quantified by the Bradford method and phenol–sulfuric acid assay, respectively (with duplicate samples)[34]. Macroscopic rheological behavior was evaluated using a TA AR-2000ex coaxial cylinder rheometer (Ø 29/32 mm, L 44 mm). Samples were pre-sheared at 500 s^{-1} for 5 min to eliminate memory effects, allowed to rest for 10 min, and then subjected to shear rate scans at 25 °C to determine yield stress, apparent viscosity, and flow index.

By integrating microscale aggregation, electrokinetic regulation, and macroscale flow behavior, this multiscale analysis provides comprehensive data support for the subsequent discussion of dewatering mechanisms.

 doi:10.20944/preprints202507.1948.v1

3. Results and Discussion

3.1. Physicochemical Characteristics of Biochars

As shown in Fig. 1a, all biochars (TB, PB, MB) exhibited broad FTIR peaks at 3000–3500 cm^{-1}, indicating –OH groups on the surface. The peak near 1600 cm^{-1} corresponds to aromatic C=O and C=C vibrations, suggesting the presence of aromatic domains. PB and MB showed stronger bands at ~1043 cm^{-1}, associated with Si–O and C–O–C bonds, and peaks near 536 cm^{-1}, indicating heteroatom residues, reflecting their more complex functional group profiles and higher interfacial reactivity than TB.

XRD results (Fig. 1b) showed a broad d_{002} peak in TB, attributed to graphitized microcrystals, while PB and MB exhibited sharp SiO_2 diffraction peaks at 25°–30°, likely from sludge-derived mineral impurities. The presence of Al-related signals in PB and MB suggests residual PAC, which may contribute to enhanced Zeta potential and floc size. N_2 adsorption-desorption isotherms (Fig. 1c-d) revealed type II curves, confirming macroporosity. Specific surface areas ranked as PB (69.02 m^2/g) > MB (11.33 m^2/g) > TB (7.35 m^2/g). All samples featured dominant macropores (>50 nm) with some mesopores, supporting rapid water transport.

In summary, PB and MB exhibited superior surface area, functional group diversity, and mineral content compared to TB, providing stronger potential for charge neutralization, adsorption bridging, and structural support in enhancing sludge dewaterability.

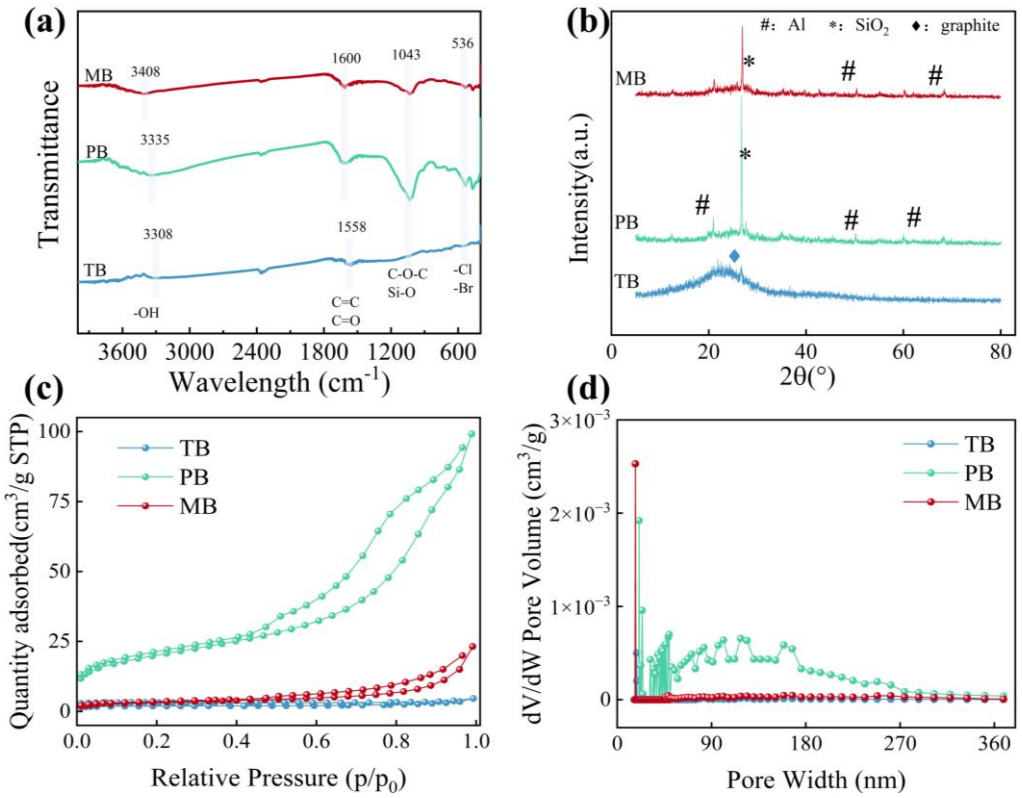

Figure 1. FTIR spectra (a), XRD patterns (b), N_2 adsorption–desorption isotherms (c), and pore-size distributions (d) of three biochars (TB, PB, MB), used to characterize surface functional groups, crystalline composition, specific surface area, and porous structure.

3.2. Sludge Dewaterability and Water Distribution Characteristics

In general, sludge with a high capillary suction time (CST) is difficult to dewater[35]. As shown in Figure S1, CST values decreased with increasing biochar dosage for all three types—tea-branch biochar (TB), PAC sludge-derived biochar (PB), and mixed biochar (MB). However, the rate of CST reduction slowed after the dosage reached 10% DS. Therefore, a dosage of 10% DS was selected for

 doi:10.20944/preprints202507.1948.v1

subsequent combined conditioning experiments. Overall, the improvement in CST by single biochar addition was less significant than that achieved by PAC or biochar-PAC combinations. This trend is further validated in Figure 2a: PAC conditioning alone reduced CST from 97.45 ± 1.91 s (raw sludge, RS) to 42.30 ± 0.85 s, while also lowering the filter cake water content (Wc) to 69.45% ± 1.79%. The combined conditioning of PAC and biochar further enhanced dewatering performance. Notably, in the TBP group, CST and Wc were reduced to 55.65 ± 1.06 s and 58.73% ± 0.40%, respectively, the best performance among all groups, achieving deep-dewatering criteria (Wc < 60%). These results suggest that PAC provides effective charge neutralization and promotes particle aggregation, while the biochar-based material acts as a skeletal support, forming a stable porous structure that facilitates deeper PAC penetration into the floc matrix, thereby enhancing its dewatering efficiency.

To further investigate the impact of different pretreatments on the water-binding characteristics in sludge, proton relaxation behavior was analyzed. As illustrated in Figure 2b, all pretreated samples exhibited short T_2 relaxation times, indicating that water-solid interactions in the sludge matrix were primarily governed by hydrogen bonding. Compared to RS, the peak areas in the T_2 distribution spectra of all treated samples were reduced to varying degrees, suggesting a general decline in water mobility. The reduction was more pronounced in biochar-treated samples, implying that biochar has a stronger effect on tightly bound water states. Moreover, in the PAC-biochar co-conditioning groups, not only was the intensity of bound water further reduced, but the T_2 peaks also shifted to the right, indicating a weakening of the water-holding capacity of microbial flocs. This enhanced the mobility of water within the sludge matrix and weakened the binding between water and solids, thereby improving dewatering performance. These observations are consistent with findings reported by Wu et al[36].

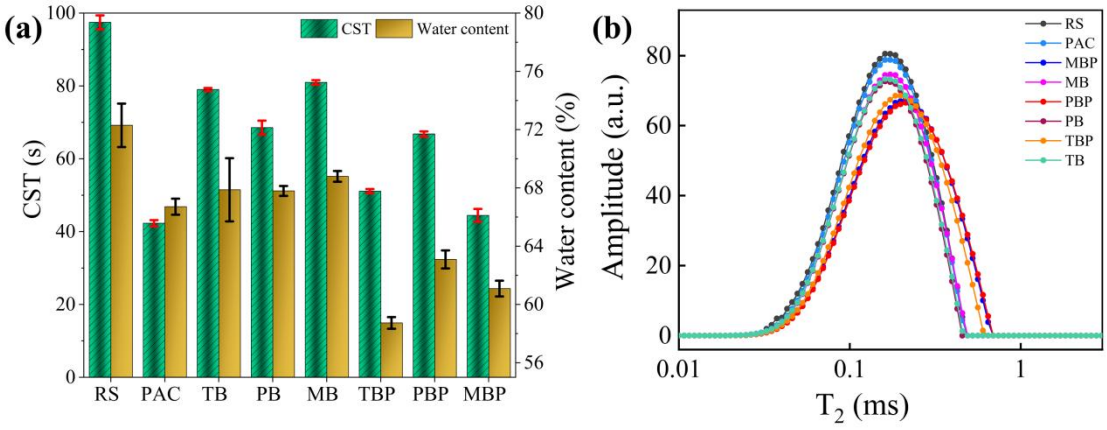

Figure 2. (a) Capillary suction time (CST) and sludge cake water content (Wc) of different sludge samples under various conditioning strategies. (b) T_2 relaxation time distribution of sludge samples obtained by low-field nuclear magnetic resonance (LF-NMR).

3.3. Changes in Physicochemical Properties of Sludge

3.3.1. Zeta Potential and Particle Size

Zeta potential is a key indicator of the surface charge status of sludge particles, reflecting the degree of electrostatic repulsion between them[37]. As shown in Figure S2, the zeta potential increases with increasing biochar dosage, although the rate of increase slows beyond 10% DS, which informed the selection of this dosage for subsequent co-conditioning. Figure 3a shows that RS exhibited a zeta potential of –25.20 ± 1.15 mV, indicating strong negative surface charges and high colloidal stability, which hinders flocculation. After conditioning with PAC, the zeta potential increased significantly to –12.53 ± 1.43 mV, demonstrating a strong electrostatic neutralization effect. In contrast, the three types of biochar (PB, MB, TB) yielded smaller increases when applied individually, with zeta potentials ranging from –21.75 to –17.72 mV. However, in the co-conditioning groups (PBP, MBP, TBP), the zeta potentials increased further to –10.98, –11.13, and –9.78 mV,

 doi:10.20944/preprints202507.1948.v1

respectively, substantially higher than with biochar alone. These results suggest that biochar not only provides limited electrostatic neutralization on its own but also enhances PAC adsorption onto sludge particles via coagulant-aiding mechanisms, thereby promoting particle destabilization and aggregation.

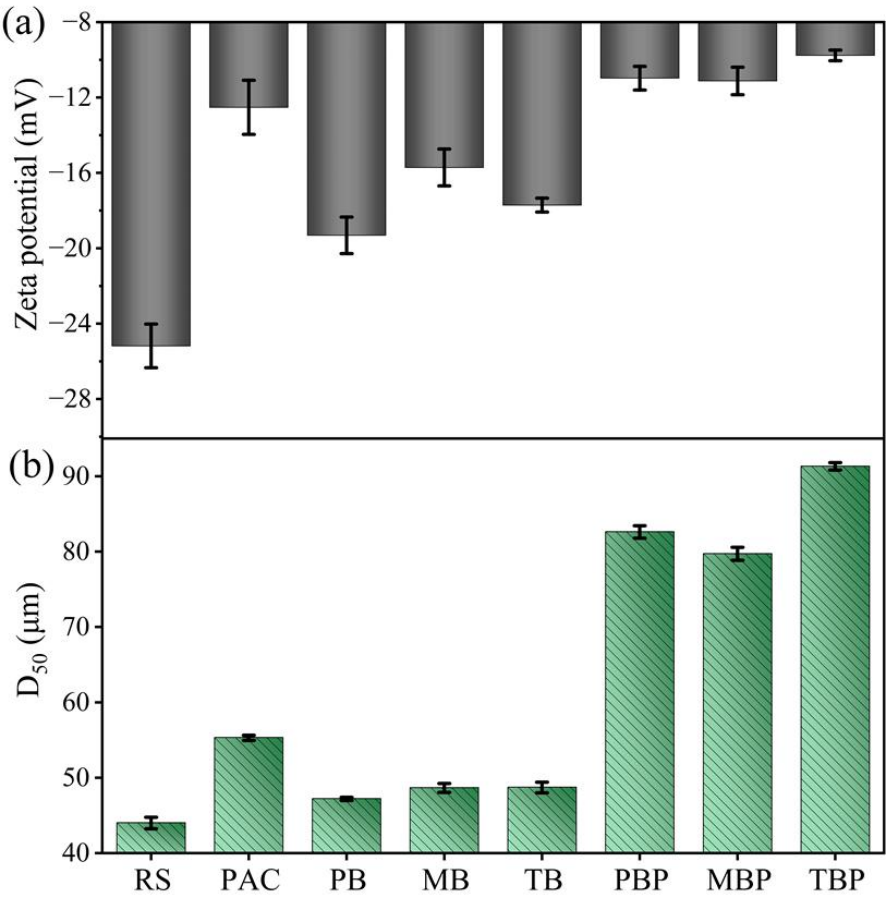

Figure 3. (a) Zeta potential and (b) average particle size (D_{50}) of sludge samples conditioned with PAC, biochars, and their combinations, determined to assess changes in electrostatic stability and floc structure.

Further analysis in Figure 3b reveals that the average particle size increased significantly following conditioning. The RS sample had an average particle size of 43.99 ± 0.76 μm, which increased to approximately 55.3 μm after PAC treatment. Slight increases were also observed in the biochar-only groups (TB: 48.70 μm; PB: 47.19 μm; MB: 48.65 μm). Notably, the particle sizes increased markedly in the co-conditioning groups: TBP reached 91.3 μm, PBP 82.6 μm, and MBP 79.7 μm, indicating strong floc-forming capacity. This enhancement is likely due to PAC supplying high-valence cations for electrostatic neutralization, while the oxygen-containing functional groups (e.g., carboxyl, hydroxyl) on the biochar surface facilitate adsorptive bridging with sludge colloids, resulting in the formation of larger particle structures. These larger flocs are beneficial for water release and solid–liquid separation.

Overall, the notable increase in zeta potential confirms that biochar strengthens the electrostatic neutralization effect of PAC. Concurrent particle size enlargement further substantiates the bridging and flocculation-enhancing role of biochar. Together, these interfacial improvements promote particle aggregation and structural openness, laying a physicochemical foundation for improved dewatering performance. These observations are consistent with the previously discussed reductions in CST and Wc, providing key mechanistic evidence, at both the charge and particle-size levels—for the effectiveness of biochar–PAC synergistic conditioning.

3.3.2. Rheological Properties

 doi:10.20944/preprints202507.1948.v1

Figure 4 and Figure S3 collectively illustrate the variations in yield stress and apparent viscosity of sludge under different conditioning strategies. As shown in Figure 4, raw sludge (RS) exhibited a yield stress of 0.039 Pa, indicating strong internal cohesion and shear resistance that hinder water release. After PAC conditioning, the yield stress decreased to 0.031 Pa. Similarly, single biochar conditioning with TB, PB, and MB reduced the yield stress to 0.032, 0.027, and 0.032 Pa, respectively, suggesting that biochar has a certain structure-loosening effect.

Notably, the combined conditioning groups (TBP, PBP, MBP) further reduced yield stress significantly to 0.024, 0.024, and 0.021 Pa, respectively. The MBP group exhibited the largest reduction, 46.2% compared to RS, indicating substantial disintegration of the floc network and an increase in slippage interfaces, thereby enhancing sludge deformability and its response to external shear.

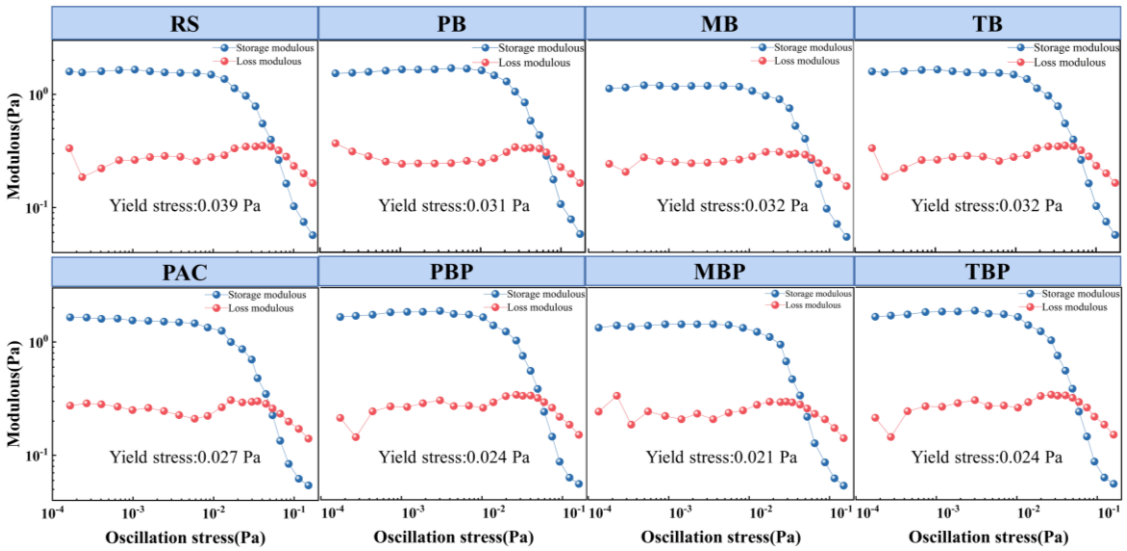

Figure 4. Yield stress of raw and conditioned sludges measured by rheometry.

Consistent with these findings, Figure S3 shows that the apparent viscosity of the sludge also decreased after conditioning. The viscosity of raw sludge was 0.027 Pa·s; this dropped to 0.021–0.024 Pa·s in the single biochar-treated groups, and further declined to 0.017 Pa·s (TBP), 0.017 Pa·s (PBP), and 0.015 Pa·s (MBP) in the co-conditioned groups. The MBP group achieved the greatest reduction, approximately 44.4% compared to RS. Additionally, as shown in the Supporting Information (SI) table, the limiting viscosity values under varying shear rates for the co-conditioned groups (5.13–5.19 mPa·s) were also lower than that of the RS group (5.37 mPa·s), further confirming the reduction in overall flow resistance.

These results demonstrate that biochar, particularly in synergy with PAC, effectively disrupts the sludge's internal structure, reduces rheological strength, and facilitates water release during mechanical dewatering.

3.3.3. EPS

Extracellular polymeric substances (EPS) play a critical role in sludge dewatering, as their composition and distribution govern floc structure and water retention[38]. As shown in Figures 5 and S4, all conditioning treatments promoted the migration of proteins (PN) and polysaccharides (PS) from tightly bound (TB-EPS) and loosely bound (LB-EPS) layers toward the soluble EPS (S-EPS) fraction. This effect was especially pronounced in PAC–biochar co-conditioning groups (TBP, PBP, MBP). In the MBP group, S-EPS PN increased from 4.19 ± 0.04 to 5.78 ± 0.10 mg/g SS, while TB-EPS PN decreased from 10.36 ± 0.22 to 7.67 ± 0.71 mg/g SS. PS exhibited a similar trend, with S-EPS rising from 0.68 ± 0.05 to 1.01 ± 0.09 mg/g SS and TB-EPS dropping from 1.86 ± 0.12 to 1.45 ± 0.07 mg/g SS. These results indicate that co-conditioning promotes EPS disintegration and redistribution. Despite these shifts, total EPS content remained relatively constant, suggesting the structural framework of

 doi:10.20944/preprints202507.1948.v1

sludge flocs was preserved. This "redistribution without degradation" maintains internal channels for water transport while weakening the gel-like binding of water within the floc.

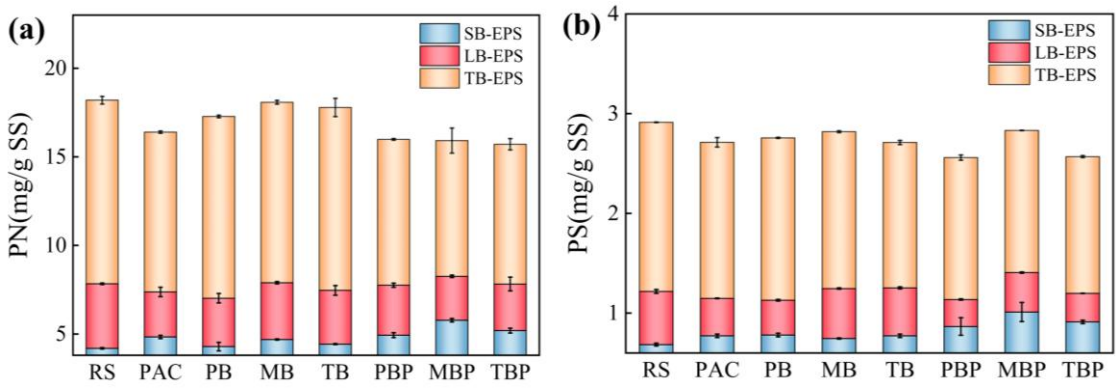

Figure 5. Protein (PN) and polysaccharide (PS) contents in different extracellular polymeric substances (EPS) fractions (TB-EPS, LB-EPS, and S-EPS) for sludge samples subjected to different conditioning treatments.

Overall, while PAC or biochar alone moderately promote EPS migration, their combination induces a stronger synergistic effect, enhancing floc looseness and compressibility. Together with zeta potential elevation, particle size growth, and rheological softening, EPS restructuring emerges as a central mechanism in improved deep dewatering, driven by PAC's charge neutralization and biochar's bridging and skeletal support.。

3.3.4. Floc Morphology and Microstructural Characteristics

To investigate the effects of different conditioning strategies on sludge floc structure, SEM was employed to visualize surface morphology and pore features (Figures 6 and S5). Pore sizes were quantified using ImageJ software. The results revealed significant differences in microstructure and porosity across treatments. RS exhibited a smooth, dense surface with minimal porosity (average pore diameter: 0.067 μm), indicative of high water retention and low permeability. PAC treatment induced structural fragmentation but only modestly increased the average pore size to 0.397 μm, with limited permeability enhancement. In contrast, biochar-treated samples (TB, PB, MB) showed substantial pore enlargement. The TB group developed a honeycomb-like architecture with pores up to 0.839 μm, reflecting biochar's capacity to provide rigid skeletal support and construct drainage channels.

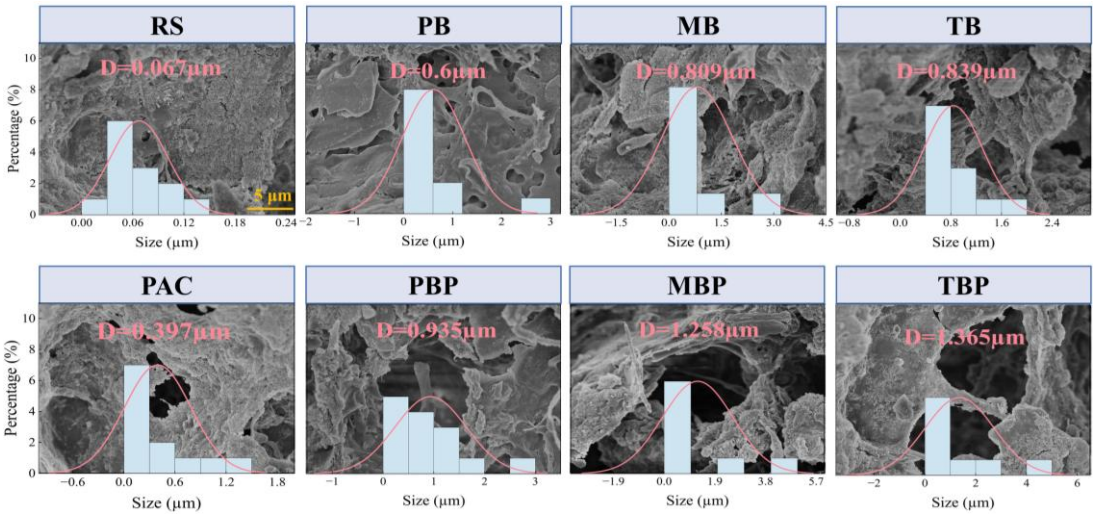

Figure 6. Scanning electron microscopy (SEM) images and quantitative pore size analysis of sludge cakes after different conditioning treatments, used to observe structural morphology and microstructural features.

 doi:10.20944/preprints202507.1948.v1

Co-conditioning with PAC and biochar (TBP, PBP, MBP) further promoted crack development and pore connectivity. The average pore diameters increased to 1.365 μm (TBP), 0.935 μm (PBP), and 1.258 μm (MBP), significantly exceeding those of single-agent treatments. High-magnification images revealed that biochar particles were embedded within the floc matrix, forming stable bridging–support networks that provided structural anchoring for PAC action and enhanced water permeability. These results confirm that biochar contributes to deep dewatering via a "skeleton support–structural loosening–channel formation" mechanism, reinforcing PAC's conditioning effect and facilitating porous network construction.

3.4. Proposed Dewatering Mechanism

Based on the results above, a comprehensive mechanism for PAC–biochar co-conditioning is proposed, as illustrated in Figure 7. The three types of biochar (TB, PB, MB) provided rigid and porous structures that acted as internal skeletons within the sludge matrix, enhancing floc mechanical stability while forming continuous pore channels that facilitated water migration during compression. This skeletal support helped preserve floc integrity and maintain drainage pathways under high pressure, contributing to improved dewatering[3]. Zeta potential measurements confirmed enhanced charge neutralization after co-conditioning, increasing from –25.20 mV to –14.99 ~ –15.72 mV, which reduced electrostatic repulsion and promoted particle aggregation. Concurrently, particle size increased substantially, up to 191.3 μm in the TBP group, due to the synergistic bridging between PAC and the oxygen-containing functional groups (e.g., hydroxyl, carboxyl) on the biochar surface. In PB and MB, the presence of SiO_2 may further enhance Al^{3+}-mediated crosslinking from PAC, leading to the formation of larger, more stable flocs. Additionally, co-conditioning significantly lowered sludge yield stress and apparent viscosity (up to 46.2% reduction), indicating enhanced compressibility and fluidity. EPS redistribution was also evident, with proteins and polysaccharides shifting from the tightly bound (TB-EPS) to the more mobile S-EPS and LB-EPS fractions. In the MBP group, S-EPS protein concentration increased to 5.78 mg/g SS, indicating weakened water-binding capacity and increased surface hydrophobicity, both of which facilitate water release.

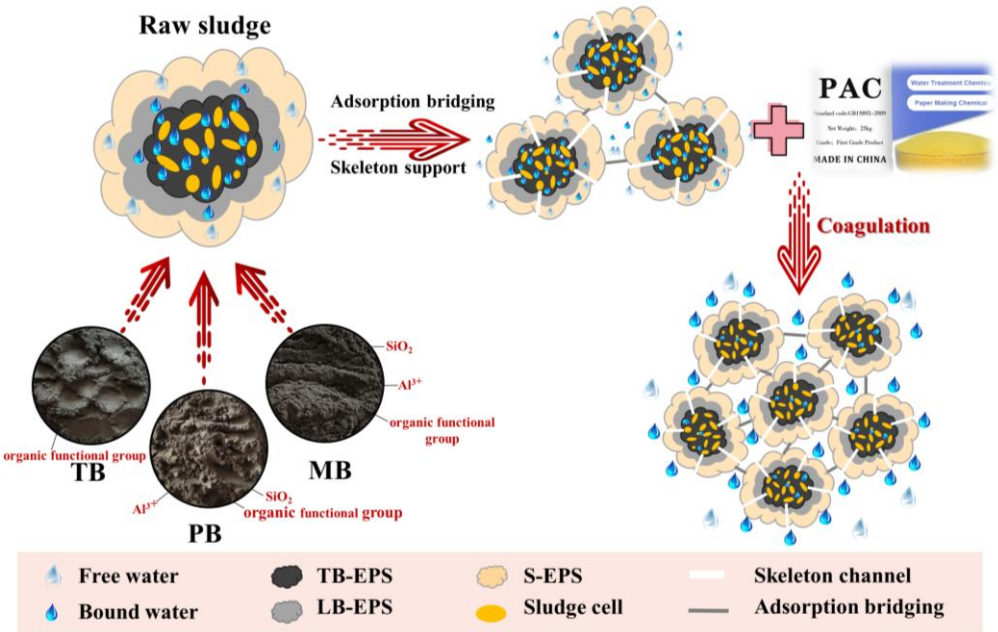

Figure 7. Conceptual schematic of the proposed sludge dewatering mechanism, illustrating the roles of biochar and PAC in structural support, charge neutralization, adsorption bridging, and EPS regulation.

 doi:10.20944/preprints202507.1948.v1

Together, these effects constitute a synergistic mechanism—skeleton support, charge neutralization, adsorptive bridging, EPS redistribution, and pore structure reconstruction, that improves sludge microstructure, interfacial properties, and colloidal stability. This integrated pathway ultimately enables efficient deep dewatering and offers a theoretical and practical foundation for developing high-performance, environmentally sustainable sludge conditioning technologies.

5. Conclusions

This study systematically evaluated the synergistic effects of three tea waste-derived biochar materials (TB, PB, MB) and their combined application with polyaluminum chloride (PAC) on the dewatering performance of municipal sludge. The results highlight the practical potential and mechanistic foundation of biochar-based skeletal materials in green sludge conditioning strategies. The main conclusions are as follows:

(1) Compared to single-agent conditioning, the combination of biochar and PAC significantly improved sludge dewaterability. Among the treatments, the TBP group achieved the best performance, reducing CST to 55.65 ± 1.06 s and filter cake water content to 58.73% ± 0.40%, meeting the deep dewatering threshold (Wc < 60%).

(2) In addition to offering limited electrostatic neutralization and bridging capacity, biochar acted as a skeleton-like filler during conditioning, constructing a stable porous framework within the sludge flocs. This structure enhanced internal permeability and mechanical integrity, thereby reinforcing PAC-induced coagulation and dewatering effects.

(3) Based on integrated physicochemical characterization and dewatering performance, the incorporation of biochar optimized the microstructure and water transport pathways of the sludge matrix. It facilitated more efficient water and organic matter release during dewatering, providing a feasible pathway toward low-energy, high-efficiency, and environmentally friendly sludge conditioning.

Supplementary Materials: The following supporting information can be downloaded at the website of this paper posted on Preprints.org.

Author Contributions: Qiang-Ying Zhang: Investigation, Visualization, Data curation, Formal analysis, Methodology, and Writing--original draft. Geng Xu, Hui-Yun Qi: Investigation and Data curation. Hou-Feng Wang: Conceptualization,Data curation, Methodology, Project administration,Writing-review and editing. Xiao-Mei Cui: Review and editing, Supervision, and Funding acquisition.

Acknowledgments: This research was funded by the Lhasa Municipal Major Science and Technology Project (No. LSKJ202543), Talent Incentive Project of Tibet University (No. ZDRC202410), Science and Technology Plan Projects of Shigatse City (No. RKZ2024ZY-06), Science and Technology projects of Xizang Autonomous Region (XZ202501ZY0072, XZ202501ZY0008), Central Financial Support Special Funds for Local Colleges and Universities (No. [2024]01, [2025]01).

References

1. L. Li, Y. Hua, S. Zhao, D. Yang, S. Chen, Q. Song, J. Gao, X. Dai, Worldwide Research Progress and Trend in Sludge Treatment and Disposal: A Bibliometric Analysis, ACS EST ENG, 3 (2023) 1083-1097.
2. W. Zheng, Y. Shao, S. Qin, Z. Wang, Future directions of sustainable resource utilization of residual sewage sludge: A review, SUSTAINABILITY-BASEL, 16 (2024) 6710.
3. P. Bao, C. Du, Y. Li, H. Jiang, L. Zhou, G. Yu, S. Sun, L. Zhou, X. Li, J. Teng, X. Wang, J. Wang, Application of skeleton builders to sludge dewatering and disposal: A critical review, SCI TOTAL ENVIRON, 906 (2024) 167106.
4. X. Zhang, P. Ye, Y. Wu, Enhanced technology for sewage sludge advanced dewatering from an engineering practice perspective: A review, J ENVIRON MANAGE, 321 (2022).

 doi:10.20944/preprints202507.1948.v1

5. J. Liang, Y. Zhou, Iron-based advanced oxidation processes for enhancing sludge dewaterability: State of the art, challenges, and sludge reuse, WATER RES, 218 (2022).
6. P. Yao, A. You, Optimization of thermal–alkaline pretreatment for dewatering of excess sludge followed by thermal/persulfate oxidation for the elimination of extracellular ARGs in TAP-treated filtrate, WATER SCI TECHNOL, 87 (2023) 2210-2222.
7. H. Pang, Y. Xu, R. Ren, J. He, X. Pan, L. Wang, Enhanced anaerobic digestion of waste activated sludge by alkaline protease-catalyzing hydrolysis: Role and significance of initial pH adjustment, CHEM ENG J, 467 (2023) 143323.
8. X. Zhang, P. Ye, Y. Wu, Enhanced technology for sewage sludge advanced dewatering from an engineering practice perspective: A review, J ENVIRON MANAGE, 321 (2022) 115938.
9. W. Hua, B. Gao, J. Ren, A. Li, H. Yang, Coagulation/flocculation in dewatering of sludge: A review, WATER RES, 143 (2018) 608-631.
10. B. Cao, T. Zhang, W. Zhang, D. Wang, Enhanced technology based for sewage sludge deep dewatering: A critical review, WATER RES, 189 (2021) 116650.
11. J. Liang, C. Le, Iron-based advanced oxidation processes for enhancing sludge dewaterability: State of the art, challenges, and sludge reuse, WATER RES, 218 (2022) 118499.
12. A. Harmaji, R. Jafari, G. Simard, Valorization of residue from aluminum industries: a review, MATERIALS, 17 (2024) 5152.
13. P. Bao, C. Du, Y. Li, H. Jiang, L. Zhang, G. Yu, S. Sun, L. Zhou, X. Li, J.T.C. Teng, X. Wang, J. Wang, Application of skeleton builders to sludge dewatering and disposal: A critical review, SCI TOTAL ENVIRON, 906 (2024) 167106.
14. Y. Jiang, F. Gao, N. Zhang, J. Li, M. Xu, Y. Jiang, Dehydration Performance of Municipal Sludge and Its Dewatering Conditioning Methods: A Review, IND ENG CHEM RES, 62 (2023) 11337-11357.
15. Y. Qi, K.B. Thapa, A.F.A. Hoadley, Application of filtration aids for improving sludge dewatering properties - A review, CHEM ENG J, 171 (2011) 373-384.
16. J. Wang, H. Liu, H. Deng, M. Jin, H. Xiao, H. Yao, Deep dewatering of sewage sludge and simultaneous preparation of derived fuel via carbonaceous skeleton-aided thermal hydrolysis, CHEM ENG J, 402 (2020) 126255.
17. K. Xiao, Y. Lv, W. Yu, J. Yang, Visualization of water transfer channel in sludge dewatering conditioned with skeleton builders by X-ray micro-computed tomography, CHEMOSPHERE, 355 (2024) 141818.
18. W. Li, W. Wang, D. Wu, S. Yang, H. Fang, S. Sun, Mechanochemical treatment with red mud added for heavy metals solidification in municipal solid waste incineration fly ash, J CLEAN PROD, 398 (2023) 136642.
19. K. Chen, Y. Sun, J. Fan, Y. Gu, The dewatering performance and cracking-flocculation-skeleton mechanism of bioleaching-coal fly ash combined process for sewage sludge, CHEMOSPHERE, 307 (2022) 135994.
20. P. Kuryntseva, K. Karamova, P. Galitskaya, S. Selivanovskaya, G. Evtugyn, Biochar functions in soil depending on feedstock and pyrolyzation properties with particular emphasis on biological properties, Agriculture, 13 (2023) 2003.
21. R. Ramos, V.K. Abdelkader-Fernández, R. Matos, A.F. Peixoto, D.M. Fernandes, Metal-supported biochar catalysts for sustainable biorefinery, electrocatalysis, and energy storage applications: a review, CATALYSTS, 12 (2022) 207.
22. S.S. Senadheera, P.A. Withana, J.Y. Lim, S. You, S.X. Chang, F. Wang, J.H. Rhee, Y.S. Ok, Carbon negative biochar systems contribute to sustainable urban green infrastructure: a critical review, GREEN CHEM, (2024).
23. H. Lei, Z. Wang, S. Li, M. Zhu, Recent advancements in chemical recycling and biodegradation of post-consumer polystyrene waste, GREEN CHEM, (2025).
24. S. Li, F. Lü, H. Zhang, L. Shao, P. He, Electron exchange capacities of colloidal biochar: Affected by spatial structure distribution instead of particle size, CHEM ENG J, 455 (2023) 140567.
25. J. Zhang, P. Li, Y. Yu, Y. Xu, W. Jia, S. Zhao, A review of natural polysaccharides-based flocculants derived from waste: application efficiency, function mechanism, and development prospects, IND ENG CHEM RES, 62 (2023) 15774-15789.

 doi:10.20944/preprints202507.1948.v1

26. B. Liu, K. Guo, Q. Yue, Y. Gao, B. Gao, Effect of Microplastics on the Coagulation Mechanism of Polyaluminum–Titanium Chloride Composite Coagulant for Organic Matter Removal Revealed by Optical Spectroscopy, ACS EST ENG, 4 (2024) 1914-1926.
27. S. Miao, Y. Wei, J. Chen, X. Wei, Extraction methods, physiological activities and high value applications of tea residue and its active components: a review, CRIT REV FOOD SCI, 63 (2023) 12150-12168.
28. Z. You, L. Zhao, K. Zhao, H. Liao, S. Wen, Y. Xiao, B. Cheng, S. Lei, Highly tunable three-dimensional porous carbon produced from tea seed meal crop by-products for high performance supercapacitors, APPL SURF SCI, 607 (2023) 155080.
29. H. Wang, H. Qi, Z. Lian, Y. Zhang, J. Li, R.J. Zeng, A unified operating procedure is crucial to evaluate sludge dewaterability, taking the setup of refrigerated storage time as an example, J ENVIRON MANAGE, 307 (2022) 114528.
30. B. Rao, J. Su, S. Xu, H. Pang, P. Xu, Y. Zhang, J. Zhu, H. Tu, Thermal and non-thermal mechanism of microwave irradiation on moisture content reduction of municipal sludge, WATER RES, 226 (2022) 119231.
31. B. Rao, J. Su, S. Xu, H. Pang, P. Xu, Y. Zhang, J. Zhu, H. Tu, Thermal and non-thermal mechanism of microwave irradiation on moisture content reduction of municipal sludge, WATER RES, 226 (2022) 119231.
32. B. Wu, H. Li, K. Zhou, N. Yu, Q. Xu, X. Chai, X. Dai, Crystallization-driven evolution of water occurrence states with implications on dewaterability improvement of waste-activated sludge, WATER RES, 244 (2023) 120496.
33. X.Y. Li, S.F. Yang, Influence of loosely bound extracellular polymeric substances (EPS) on the flocculation, sedimentation and dewaterability of activated sludge, WATER RES, 41 (2007) 1022-1030.
34. W. Yu, J. Yang, Y. Shi, J. Song, Y. Shi, J. Xiao, C. Li, X. Xu, S. He, S. Liang, Roles of iron species and pH optimization on sewage sludge conditioning with Fenton's reagent and lime, WATER RES, 95 (2016) 124-133.
35. W. Liu, H. Zhang, Y. Zhang, P. Sun, Y. Zeng, Y. Gao, H. Wang, R.J. Zeng, Beyond filterability: Understanding the complexities of sludge dewatering through typical coagulation and advanced oxidation, J CLEAN PROD, 429 (2023) 139520.
36. B. Wu, H. Wang, Y. He, X. Dai, B. Wu, Influential mechanism of water occurrence states of waste-activated sludge: Over-focused significance of cell lysis to bound water reduction, WATER RES, 221 (2022) 118737.
37. Y. Li, D. Wang, G. Yang, X. Yuan, Q. Xu, Q. Yang, Y. Liu, Q. Wang, B. Ni, W. Tang, L. Jiang, Enhanced dewaterability of anaerobically digested sludge by in-situ free nitrous acid treatment, WATER RES, 169 (2020).
38. W. Yu, Q. Wen, J. Yang, K. Xiao, Y. Zhu, S. Tao, Y. Lv, S. Liang, W. Fan, S. Zhu, B. Liu, H. Hou, J. Hu, Unraveling oxidation behaviors for intracellular and extracellular from different oxidants (HOCl vs. H2O2) catalyzed by ferrous iron in waste activated sludge dewatering, WATER RES, 148 (2019) 60-69.